

1 **Somatic uniparental disomy mitigates the most damaging *EFL1* allele**
2 **combination in Shwachman-Diamond syndrome**

3

4 Sangmoon Lee^{1,*}, Chang Hoon Shin^{2,*}, Jawon Lee¹, Seong Dong
5 Jeong², Che Ry Hong³, Jun-Dae Kim⁴, Ah-Ra Kim⁵, Soo Jin Son^{6,7},
6 Oleksandr Kokhan⁸, Taekyeong Yoo¹, Jae Sung Ko³, Young Bae Sohn⁹, Ok-
7 Hwa Kim¹⁰, Jung Min Ko³, Tae-Joon Cho¹¹, Nathan T. Wright⁸, Je Kyung
8 Seong^{6,7,12}, Suk-Won Jin^{4,5}, Hyoung Jin Kang^{3,13,**}, Hyeon Ho Kim^{2,14,**},
9 Murim Choi^{1,3,**}

10

11 ¹Department of Biomedical Sciences, Seoul National University College of
12 Medicine, Seoul, Republic of Korea.

13 ²Department of Health Sciences and Technology, Samsung Advanced
14 Institute for Health Sciences and Technology, Sungkyunkwan University,
15 Seoul, Republic of Korea.

16 ³Department of Pediatrics, Seoul National University College of Medicine,
17 Seoul, Republic of Korea.

18 ⁴Yale Cardiovascular Research Center, Section of Cardiovascular Medicine,
19 Department of Internal Medicine, Yale University School of Medicine, New
20 Haven, CT, USA.

21 ⁵School of Life Sciences, Gwangju Institute of Science and Technology,
22 Gwangju, Republic of Korea.

23 ⁶Laboratory of Developmental Biology and Genomics, Research Institute for
24 Veterinary Science, and BK21 PLUS Program for Creative Veterinary
25 Science Research, College of Veterinary Medicine, Seoul National
26 University, Seoul, Republic of Korea.

27 ⁷Korea Mouse Phenotyping Center (KMPC), Seoul National University,
28 Seoul, Republic of Korea.

29 ⁸Department of Chemistry and Biochemistry, James Madison University,
30 Harrisonburg, VA, USA.

31 ⁹Department of Medical Genetics, Ajou University Hospital, Ajou University
32 School of Medicine, Suwon, Republic of Korea.

33 ¹⁰Department of Pediatric Radiology, VIC 365 Children's Hospital, Incheon,
34 Republic of Korea.

35 ¹¹Department of Orthopaedic Surgery, Seoul National University College of
36 Medicine, Seoul, Republic of Korea.

37 ¹²Interdisciplinary Program for Bioinformatics, Program for Cancer Biology
38 and BIO-MAX/N-Bio Institute, Seoul National University, Seoul, Republic of
39 Korea.

40 ¹³Seoul National University Cancer Research Institute, Seoul, Republic of
41 Korea.

42 ¹⁴Institute for Future Medicine, Samsung Medical Center, Seoul, Republic of
43 Korea

44

45 *S. Lee, and C.H. Shin contributed equally to this paper.

46 ** H.J. Kang, H.H.Kim, and M.Choi contributed equally to this paper

47 Correspondence to Murim Choi: murimchoi@snu.ac.kr; or Hyeon Ho Kim:

48 hyeonhkim@skku.edu or Hyoung Jin Kang: kanghj@snu.ac.kr

49

50 ¹⁵Current address: Sangmoon Lee (Department of Neurosciences,

51 University of California, San Diego, La Jolla, CA 92093, USA). Chang Hoon

52 Shin (Laboratory of Genetics and Genomics, National Institute on Aging

53 Intramural Research Program, National Institutes of Health, Baltimore, MD

54 21224, USA).

55

56 **Abstract**

57 Shwachman-Diamond syndrome (SDS; OMIM: #260400) is caused by
58 variants in *SBDS* (Shwachman-Bodian-Diamond syndrome gene), which
59 encodes a protein that plays an important role in ribosome assembly.
60 Recent reports suggest that recessive variants in *EFL1* are also responsible
61 for SDS. However, the precise genetic mechanism that leads to *EFL1*-
62 induced SDS remains incompletely understood. Here we present three
63 unrelated Korean SDS patients that carry biallelic pathogenic variants in
64 *EFL1* with biased allele frequencies, resulting from a bone marrow-specific
65 somatic uniparental disomy (UPD) in chromosome 15. The recombination
66 events generated cells that were homozygous for the relatively milder
67 variant, allowing for the evasion of catastrophic physiological consequences.
68 Still, the milder *EFL1* variant was solely able to impair 80S ribosome
69 assembly and induce SDS features in cell line, zebrafish, and mouse
70 models. The loss of *EFL1* resulted in a pronounced inhibition of terminal
71 oligo-pyrimidine element-containing ribosomal protein transcript 80S
72 assembly. Therefore, we propose a more accurate pathogenesis
73 mechanism of *EFL1* dysfunction that eventually leads to aberrant
74 translational control and ribosomopathy.

75 **Introduction**

76

77 Patients clinically diagnosed with Shwachman-Diamond syndrome (SDS;
78 OMIM: #260400) present with a constellation of disorders, such as
79 hematologic manifestations, exocrine pancreatic dysfunction with fatty
80 infiltration, and skeletal dysplasia that results in short stature¹⁻³. The
81 hematologic manifestations include neutropenia or, less severely,
82 thrombocytopenia and anemia with a predisposition for myelodysplastic
83 syndrome and acute myeloid leukemia transformations^{4,5}. Variants in *SBDS*
84 (Shwachman-Bodian-Diamond syndrome gene), which encodes a protein
85 that plays an important role in ribosome assembly, are mainly responsible
86 for the disease^{1,6-8}. Thus, SDS is considered to be a ribosomopathy, which is
87 a collective term that is used to describe a group of congenital disorders
88 caused by problems in ribosome biogenesis, assembly or function⁹.
89 Moreover, ~10% of clinically diagnosed SDS cases do not contain any
90 pathogenic *SBDS* variants, suggesting the existence of additional genetic
91 mechanisms that lead to the disorder^{1,6}. Recent reports demonstrate that
92 variants in genes other than *SBDS*, namely *EFL1*, *DNAJC21*, and *SRP54*,
93 are implicated with bone marrow failure syndrome and SDS¹⁰⁻¹⁵.
94 Homozygous variants of *EFL1* cause an SDS-like syndrome in a recessive
95 manner, which is highlighted by the observation that three of the seven
96 reported kindreds underwent consanguineous marriages^{10,11,15}. *EFL1*
97 directly interacts with *SBDS* to release eukaryotic translation initiation factor

98 6 (eIF6) from the 60S ribosomal subunit for 80S ribosomal assembly^{7,16}.

99 Thus, it needs to be further investigated whether there is an additional
100 genetic mechanism that leads to SDS in outbred populations other than
101 through homozygous pathogenic variants in *EFL1*.

102 As more human genomes with or without clinical significances
103 continue to be sequenced, it has become clear that variants of unknown
104 significances (VUS) pose a substantial obstacle in the interpretation of
105 genotype-phenotype relationships. As many variants are believed to
106 possess the ability to cause alternations at the molecular level but only with
107 sub-clinical levels of severity, numerous scenarios that enable VUS to
108 acquire clinical significances have been postulated. One of these scenarios
109 involves the assessment of somatically acquired uniparental disomy (UPD)
110 in the hematopoietic system; although only a small number of instances
111 have been previously reported. Notable examples include myeloid
112 neoplasia^{17,18}, immunodeficiency¹⁹, and a single case of sickle cell
113 disease²⁰.

114 In this study, we demonstrated a disease-causing mechanism in
115 patients who inherited compound heterozygous variants in *EFL1*. A mosaic
116 UPD caused a loss-of-heterozygosity (LOH) in the *EFL1* locus in the bone
117 marrow and blood, simultaneously homozygosing the less damaging variant
118 and decreasing the representation of the more damaging variant to avoid
119 worse hematologic phenotypes. However, this still led to *EFL1* dysfunction
120 in the bone marrow and resulted in SDS features. We further demonstrated

121 that the remaining variant by the UPD was a hypomorph and pathogenic, by
122 investigating the molecular mechanism of the EFL1 dysfunction in cell and
123 animal models. Therefore, searching for a pathogenic variant that was
124 caused by a non-conventional pathway may increase the probability of
125 identifying the genetic cause and improve our understanding of the disease
126 mechanism, and this approach could possibly benefit additional patients
127 with severe hematological abnormalities.

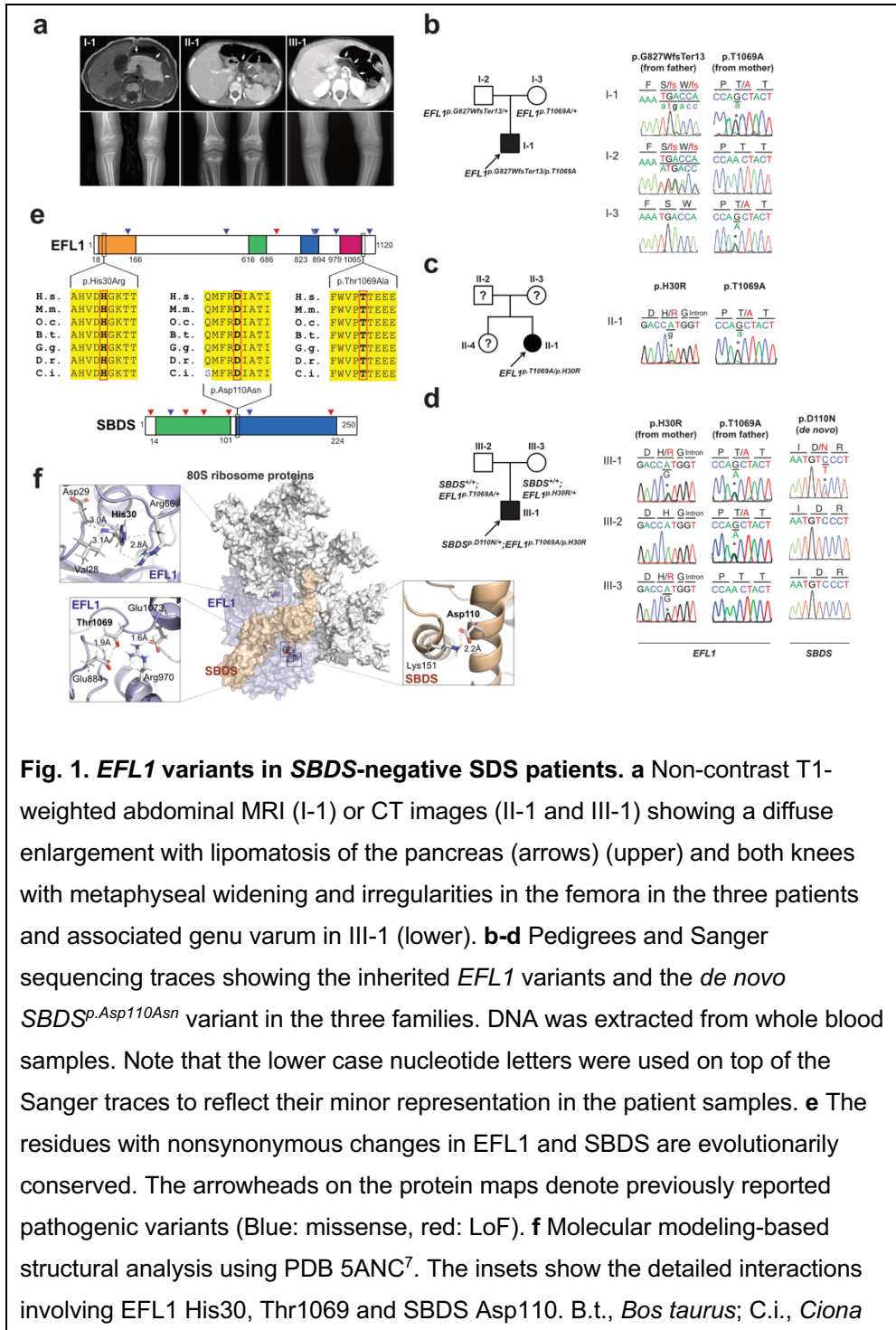
128

129 **Results**

130

131 **Shwachman-Diamond syndrome patients without *SBDS* variants**

132 We recruited three unrelated and non-consanguineous Korean SDS patients
133 without plausible recessive mutations in *SBDS* (Fig. 1a; Table S1;
134 Supplemental Clinical Narratives). Proband I-1 is a 3-year-old boy who had
135 severe intrauterine growth retardation that resulted in a preterm delivery
136 (35+3 weeks) and a birth weight of 1.7 kg. He had thrombocytopenia,
137 neutropenia, and anemia at 2-months of age. A bone marrow examination
138 performed at 6-months of age revealed hypocellularity, reduced
139 megakaryocytes, and an increase in iron storage. He also had pancreatic
140 lipomatosis, along with an exocrine pancreatic insufficiency, and
141 metaphyseal chondrodysplasia (Fig. 1a; Fig. S1). Proband II-1 is a 9-year-
142 old female who had severe intrauterine growth retardation that resulted in a
143 preterm delivery (36 weeks) and a birth weight of 1.6 kg. She had a diffuse
144 fatty infiltration of the pancreas and metaphyseal chondrodysplasia that was
145 accompanied by osteopenia and short stature (Fig. 1a). Her sister was
146 unaffected. Proband III-1 is a 25-year-old male who did not have any
147 perinatal problems except for a low birth weight (40+4 weeks, 2.4 kg). At 2-
148 years-old, he had pancreatic exocrine and endocrine insufficiencies,
149 thrombocytopenia, anemia, intermittent neutropenia, metaphyseal
150 chondrodysplasia, and ichthyosis. Later, he developed osteoporosis,
151 hepatomegaly, and a total fatty change of the pancreas (Fig. 1a).



intestinalis; D.m., *Drosophila melanogaster*; D.r., *Danio rerio*; G.g., *Gallus gallus*; H.s., *Homo sapiens*; M.m., *Mus musculus*; O.c., *Oryctolagus cuniculus*.

152

153 **Identification of mosaic *EFL1* variants**

154 To identify the genetic factors that predisposed the three patients to SDS,
155 we exome-sequenced the patients and the available parental DNA was
156 extracted from whole blood (Table S2). Notably, the heterozygous
157 p.Thr1069Ala variant of *EFL1* (chr15:82,422,872 T>C, hg19,
158 NM_024580.5:c.3205A>G) was identified in all three patients (Fig. 1b-d,
159 Table 1; Table S3), which was not previously found in SDS patients. Based
160 on gnomAD, it is a low frequency variant that was carried by three
161 individuals among 17,972 alleles in the East Asian population (East Asian
162 allele frequency (EA-AF) = 1.7×10^{-4})²¹. Under the assumption that *EFL1*
163 variants function in a recessive manner, we sought to ascertain additional
164 variants that may pose increased damage to the gene function. Remarkably,
165 we found a second variants in *EFL1* in all three patients which were not
166 detected by the initial analysis either due to a low number of variant
167 supporting reads in the proband or due to a low mapping quality caused by
168 the sequence similarity between the *EFL1* and *EFL1P1* loci. Proband I-1
169 carried a paternally-originated frameshift variant p.Gly827TrpfsTer13
170 (chr15:82,444,316 C>CA, hg19, NM_024580.5:c.2478dupT, gnomAD EA-
171 AF = 0) with a minor allele frequency (MAF) of 8.3%, and Proband II-1 and
172 III-1 carried an inherited missense variant p.His30Arg (chr15: 82,554,031
173 T>C, hg19, NM_024580.5:c.89A>G, gnomAD EA-AF = 5.1×10^{-5}) with

174 MAFs of 14.8% and 36.8%, respectively (Table 1). In addition, Proband III-1
175 harbored a heterozygous *SBDS* p.Asn110Asp variant as *de novo* (Fig. 1d;
176 Fig. S2), which is never seen in the control databases. Then we noted that
177 the non-reference allele of *EFL1* p.Thr1069Ala for I-1 and II-1 was
178 dominantly covered compared to the reference allele (Table 1), which
179 caused it to function like an incomplete homozygous variant, while the ratio
180 was comparable in III-1 (Fig. 1c; Table 1). All the *EFL1* variants were equally
181 represented in the parental carriers. The patients did not carry any variant in
182 other SDS-associated genes, including *DNAJC21* and *SRP54* (data not
183 shown). The two *EFL1* amino acid residues harboring the missense variants
184 (His30 and Thr1069) are highly conserved throughout evolution and are
185 predicted to be pathogenic (Fig. 1e; Table S4). The protein structure
186 analysis suggested that the His30 and Thr1069 residues form hydrogen
187 bonds with neighboring residues, which would presumably confer stability to
188 the protein structure. Notably, previously reported pathogenic residues
189 Cys883 and Arg970 lie close to Thr1069 (Fig. 1f; Fig. S3)¹⁵. The *SBDS*
190 Asn110 residue is also conserved among the vertebrate species (Fig. 1e;
191 Table S4) and is expected to interact with neighboring amino acids,
192 including Lys151 (Fig. 1f).

193 To understand the genetic cause of this observation, we
194 investigated whether large-scale structural variants exist that encompass
195 the region. Indeed, all the patients carried a partial LOH in chromosome 15,
196 where *EFL1* resides (Fig. 2a; Figs. S4 and S5). This LOH was copy-neutral

197 and was not seen in the healthy parents (Fig. S6), suggesting that it was
198 caused by a somatic UPD. This LOH of the *EFL1* locus is not frequently
199 found in healthy Korean individuals ($1/3,667 = 2.7 \times 10^{-4}$, Fig. S7). Also,
200 according to a survey of hematopoietic chromosomal mosaicism events, 117
201 of 151,202 apparently normal individuals carry a copy-neutral LOH or a
202 copy-number deletion of the *EFL1* locus (7.7×10^{-4})²². Thus, the LOH of the
203 *EFL1* locus is a rare event. The sizes of the LOH intervals were variable
204 among the patients (100%, 100% and 27.8% of the entire chromosome
205 span for I-1, II-1, and III-1, respectively; Fig. 2a). We also sought to identify
206 the haplotype origins of the variants that the probands carried and observed
207 that the chromosomes that were dominantly represented (*i.e.*, the maternal
208 chromosome for I-1 and the paternal chromosome for III-1) harbored
209 *EFL1*^{p.Thr1069Ala}, which was consistent with their higher coverage ratios
210 compared to other variants as documented in the WES analysis (Fig. 2a). To
211 test if the UPD event occurred in a mosaic pattern and whether LOH-
212 carrying and non-LOH-carrying cells co-exist, a single-cell SNP microarray
213 experiment was performed using bone marrow (I-1) or cells from buccal
214 swabs (III-1). As expected, complete LOHs in chromosome 15 were
215 observed in a subset of the cells, confirming the mosaic UPD events that
216 preferentially selected *EFL1*^{p.Thr1069Ala} over the other variants (*i.e.*,
217 *EFL1*^{p.Gly827TrpfsTer13} and *EFL1*^{p.His30Arg}; Fig. 2b-d; Fig. S8). Therefore, cells
218 containing UPD of chromosome 15 are expected to be homozygous for the
219 *EFL1*^{p.Thr1069Ala} allele and be a homozygous reference for the other two

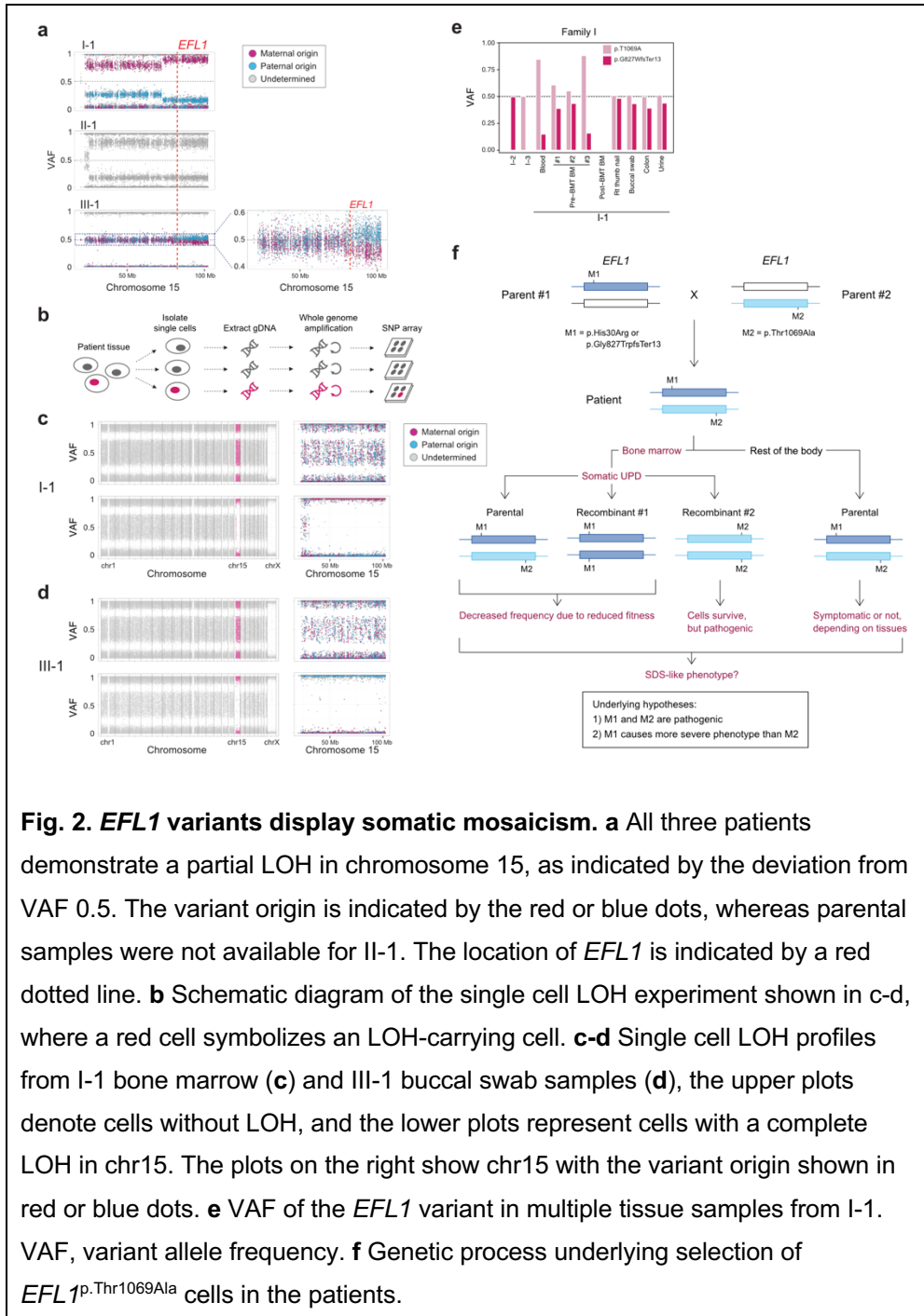


Fig. 2. *EFL1* variants display somatic mosaicism. **a** All three patients demonstrate a partial LOH in chromosome 15, as indicated by the deviation from VAF 0.5. The variant origin is indicated by the red or blue dots, whereas parental samples were not available for II-1. The location of *EFL1* is indicated by a red dotted line. **b** Schematic diagram of the single cell LOH experiment shown in c-d, where a red cell symbolizes an LOH-carrying cell. **c-d** Single cell LOH profiles from I-1 bone marrow (**c**) and III-1 buccal swab samples (**d**), the upper plots denote cells without LOH, and the lower plots represent cells with a complete LOH in chr15. The plots on the right show chr15 with the variant origin shown in red or blue dots. **e** VAF of the *EFL1* variant in multiple tissue samples from I-1. VAF, variant allele frequency. **f** Genetic process underlying selection of *EFL1*^{p.Thr1069Ala} cells in the patients.

221 alleles. I1-1 was not tested, because the sample was unavailable. Next, we
222 checked the spatial extent of the mosaic UPD by subjecting all available
223 tissue samples from I-1 to a high-depth amplicon sequencing analysis
224 (>10,000X coverage depths). Variant AFs of p.Thr1069Ala in I-1 were ~0.85
225 in the peripheral blood and bone marrow but ~0.5 in most tissues.
226 Conversely, AFs of p.Gly827TrpfsTer13 in the peripheral blood and bone
227 marrow were ~0.15 and displayed complementary frequencies to those of
228 p.Thr1069Ala (Fig. 2e). This observation suggested that the mosaic UPD
229 was restricted at least to the bone marrow. These results were concordant
230 with the Sanger sequencing results (Figs. S9-10). The degree of mosaicism
231 in the bone marrow tissue changed dynamically over the time course of I-1,
232 but did not strongly correlate with the clinical status of the patient (Fig. S11).
233 These results suggest that compound heterozygous variants that may
234 disable *EFL1* function and impair cell survival formed a cellular environment
235 such that cells with (less damaging) recombinant alleles gained survival
236 advantages over the parental ones (Fig. 2f).

237

238 ***EFL1* deficiency impairs 80S ribosome assembly**

239 Our interpretation of the genetic analysis assumes that the *EFL1* variants
240 are pathogenic, and harbor a gradient of severity (Fig. 2f). More specifically,
241 p.His30Arg possesses a comparable severity with the frameshift variant
242 (p.Gly827TrpfsTer13), and these two are more severe than p.Thr1069Ala.
243 To test this, we measured ribosome assembly function in the presence of

244 the *EFL1* variants, as *EFL1* is known to mediate GTP hydrolysis-coupled
245 release of eukaryotic translation initiation factor 6 (eIF6) together with SBDS
246 during the maturation of the 60S ribosome subunit^{7,15,16}. Thus, we monitored
247 the ribosomal assembly status of the wild type, siRNA-, or CRISPR/Cas9-
248 mediated ablation of *EFL1* (*EFL1*^{KD} or *EFL1*^{-/-}) in HeLa and K562 cell lines
249 to further elucidate the molecular function of the mutant protein (Fig. 3a; Fig.
250 S12). Polysome profiling of the *EFL1*^{KD} and *EFL1*^{-/-} cells showed a
251 significantly reduced 80S peak (Fig. 3b-c; Fig. S12). This abnormal
252 polysome profile was completely rescued after the introduction of FLAG-
253 tagged wild type *EFL1* but not by the clones that harbored the mutations
254 (Fig. 3b-c; Fig. S13). Interestingly, *EFL1*^{p.His30Arg} failed to rescue the mutant
255 phenotype, whereas *EFL1*^{p.Thr1069Ala} displayed a moderate effect on
256 ribosome assembly. These results indicated that *EFL1* plays a crucial role in
257 ribosome assembly, and *EFL1*^{p.His30Arg} possesses a null function, while
258 *EFL1*^{p.Thr1069Ala} is hypomorphic.

259

260 **Molecular mechanism of *EFL1*-mediated SDS pathogenesis**

261 Next, we explored the molecular function of the variants in ribosome
262 assembly. Variant function was not mediated via phosphorylation of
263 Thr1069, aberrant subcellular localization of *EFL1*, or changes in binding
264 affinity to SBDS (Fig. S14). Next, since the release of eIF6 from 60S is a
265 crucial step for 80S assembly and is mediated by SBDS-*EFL1*, we
266 investigated eIF6 level changes by altering *EFL1*. The assessment of eIF6

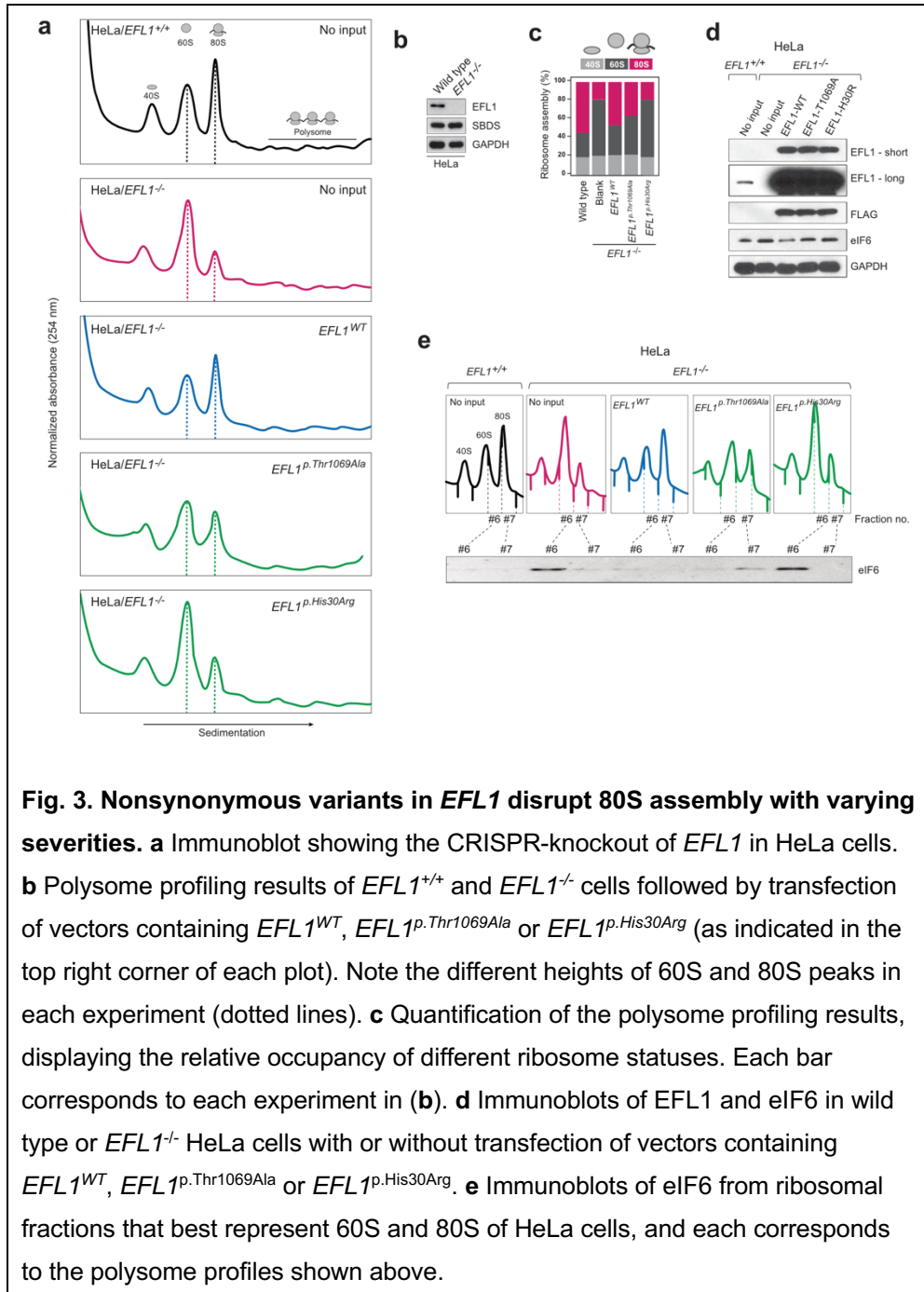


Fig. 3. Nonsynonymous variants in *EFL1* disrupt 80S assembly with varying severities. **a** Immunoblot showing the CRISPR-knockout of *EFL1* in HeLa cells. **b** Polysome profiling results of *EFL1*^{+/+} and *EFL1*^{-/-} cells followed by transfection of vectors containing *EFL1*^{WT}, *EFL1*^{p.Thr1069Ala} or *EFL1*^{p.His30Arg} (as indicated in the top right corner of each plot). Note the different heights of 60S and 80S peaks in each experiment (dotted lines). **c** Quantification of the polysome profiling results, displaying the relative occupancy of different ribosome statuses. Each bar corresponds to each experiment in (b). **d** Immunoblots of *EFL1* and eIF6 in wild type or *EFL1*^{-/-} HeLa cells with or without transfection of vectors containing *EFL1*^{WT}, *EFL1*^{p.Thr1069Ala} or *EFL1*^{p.His30Arg}. **e** Immunoblots of eIF6 from ribosomal fractions that best represent 60S and 80S of HeLa cells, and each corresponds to the polysome profiles shown above.

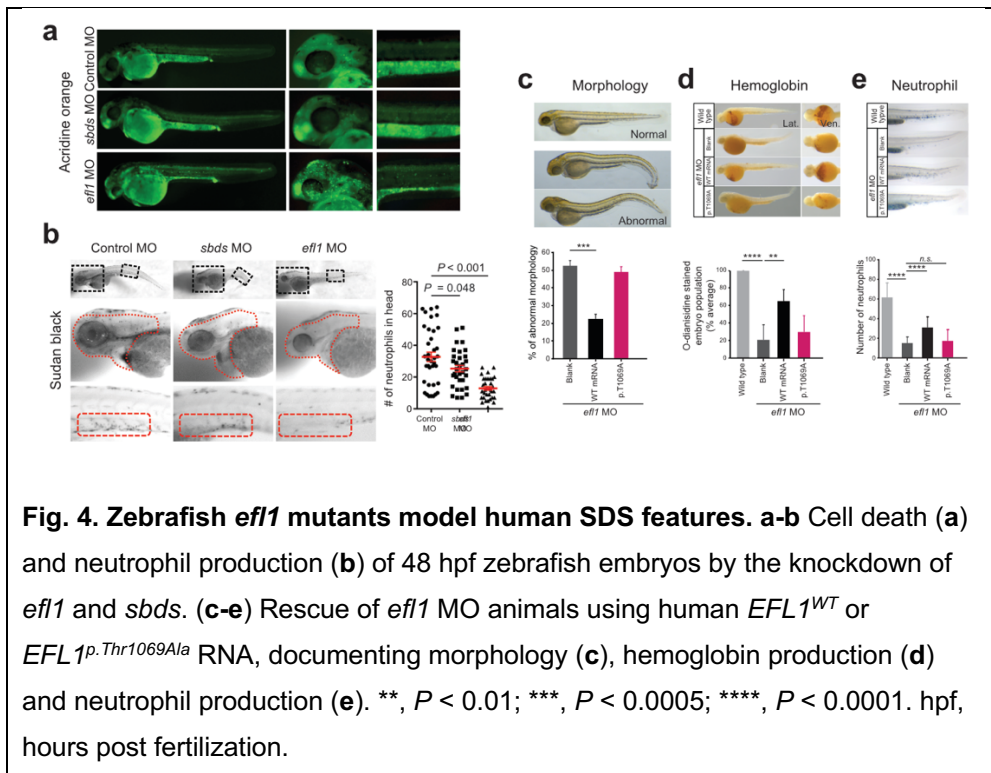
268 in wild type and *EFL1*^{-/-} cells revealed that the absence of *EFL1* induced
269 eIF6 levels, which was partially rescued by the introduction of *EFL1*^{p.Thr1069Ala}
270 or *EFL1*^{p.His30Arg} (Fig. 3d). Immunoblot analysis of each ribosomal subunit-
271 bound fraction revealed that eIF6 was more highly enriched in 60S ribosome
272 fraction of the *EFL1*^{-/-} cells as compared to the wild type or *EFL1*-
273 overexpressed cells (Fig. 3e). Remarkably, introduction of *EFL1*^{p.Thr1069Ala}
274 rescued the increased eIF6 in the 60S fraction, whereas *EFL1*^{p.His30Arg} failed
275 to do so (Fig. 3e; Fig. S15). Also, absence of *EFL1* caused an impaired
276 shuttling of cytoplasmic eIF6 back to the nucleus, consistent with the
277 previous observation (Fig. S16)¹⁵. This result, along with the observation
278 that changes in eIF6 and SBDS were not due to transcription levels (Fig.
279 S17), implies that the blocked exclusion of eIF6 and SBDS from the 60S
280 ribosomal subunit is one of the mechanisms by which our mutant protein
281 functions, which results in impaired 80S ribosome assembly. This result also
282 supports our hypothesis that the severity of p.His30Arg is higher than that of
283 p.Thr1069Ala.

284

285 **Deficiency of *EFL1* orthologs reproduces SDS phenotypes in zebrafish** 286 **and mouse models**

287 To determine whether the milder allele (*EFL1*^{p.Thr1069Ala}) was still pathogenic
288 enough to cause SDS, a morpholino-targeting zebrafish model of *efl1* was
289 subjected to rescue experiments (Fig. S18). The *efl1* morphants had smaller
290 heads and eyes as well as slightly bent tails and displayed an increased

291 number of apoptotic cells during development (Fig. 4a). Also, primitive
 292 erythrocytes and granulocytes were significantly reduced in the *eff1*

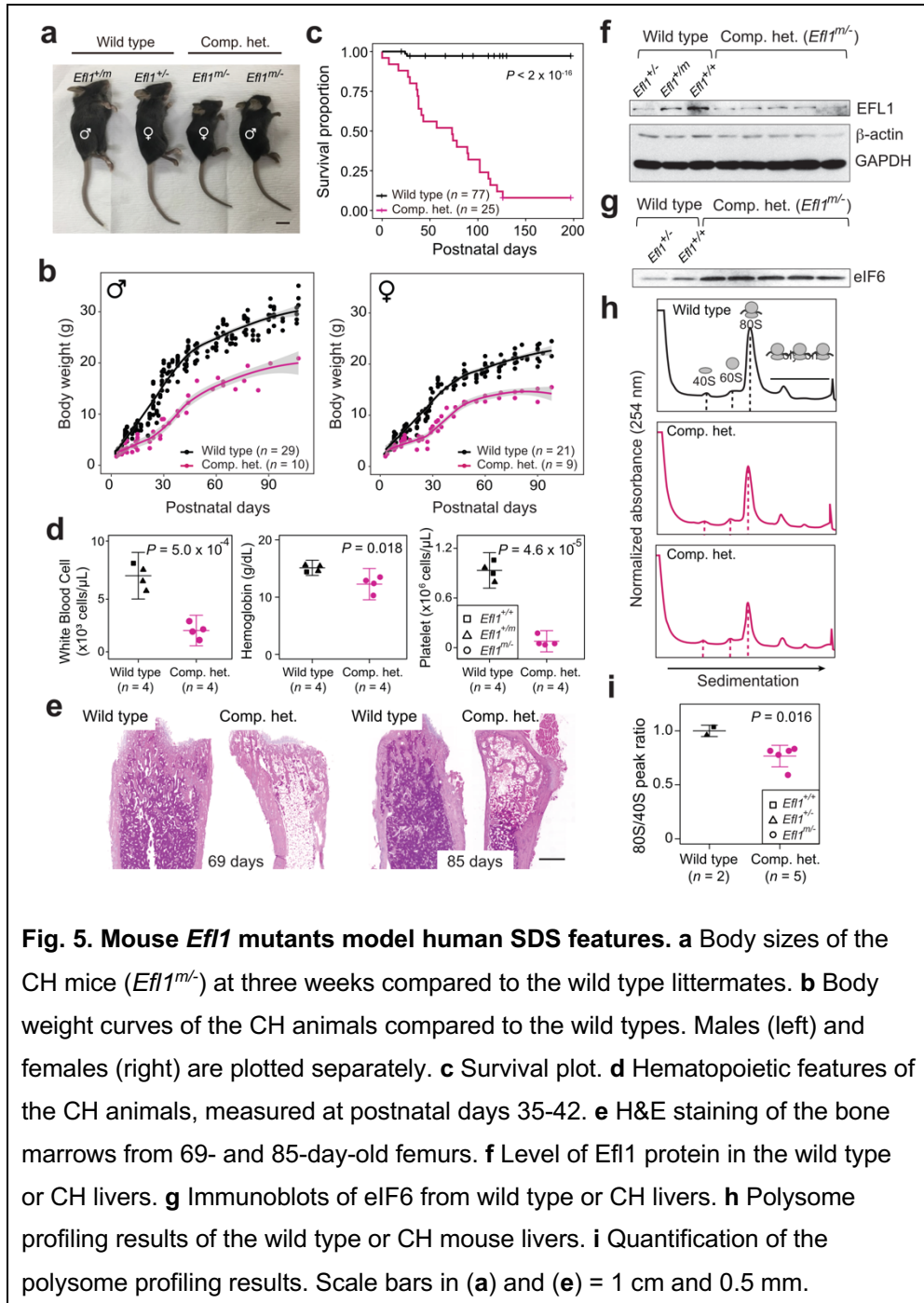


293
 294 morphants, indicating impaired primitive hematopoiesis in these embryos
 295 (Fig. 4a-b). All phenotypes were rescued by the introduction of the wild type
 296 human *EFL1* mRNA, but less so by the *EFL1*^{p.Thr1069Ala} mRNA (Fig. 4c-e),
 297 confirming that the milder *eff1* allele caused SDS-like features in zebrafish.

298 In addition, mouse models were created to further investigate the
 299 impact of *Efl1* dysfunction. *Efl1* knock-out and p.Thr1076Ala knock-in mice
 300 (mouse Thr1076 is orthologous to human Thr1069; herein designated as
 301 *Efl1*^m) were generated and subjected to phenotypic analyses (Fig. S19).
 302 Embryos that were homozygous for the null allele (*Efl1*^{-/-}) were not retrieved

303 on embryonic day (E) 8.5, implying the essential requirement of the gene in
304 early embryogenesis (Fig. S19). On the other hand, mice homozygous for
305 the knock-in allele (*Efl1^{m/m}*) were viable and healthy (Fig. S19), indicating a
306 differential phenotypic tolerance between mice and humans. To model an
307 accurate *Efl1* dose that may induce an SDS-like phenotypic expression, we
308 inter-crossed the two strains and compared phenotypes of the compound
309 heterozygous (CH) animals (*Efl1^{m/-}*) to the littermates (*Efl1^{+/+}*, *Efl1^{+/-}* and
310 *Efl1^{+/m}*), with an emphasis on the major SDS symptoms. The CH mice were
311 smaller (Fig. 5a-b) and died earlier (Fig. 5c). The blood counts revealed
312 reduced hemoglobin, white blood cells and platelets (Fig. 5d), and the bone
313 marrow images displayed a consistent deficiency (Fig. 5e). These results
314 validated our observation that the reduced function of the *EFL1^{p.Thr1069Ala}*
315 variant caused SDS in human patients. To determine whether *Efl1*
316 expression was affected by the *Efl1^m* variant, we measured the protein
317 expression from E17.5 livers (Fig. 5f). The liver heterozygous for *Efl1^m*
318 (*Efl1^{+/m}*) showed reduced *Efl1* expression, suggesting that the variant not
319 only reduced *Efl1* activity, but also destabilized the protein. The expression
320 of eIF6 was also detected in the CH livers and was increased compared to
321 the wild type livers, which was consistent with our previous observation in
322 the HeLa cells (Fig. 5g). Ribosome profiling of the wild type and CH livers
323 revealed that the CH livers showed a lower 80S peak compared to the wild
324 type livers (Fig. 5h-i).

325



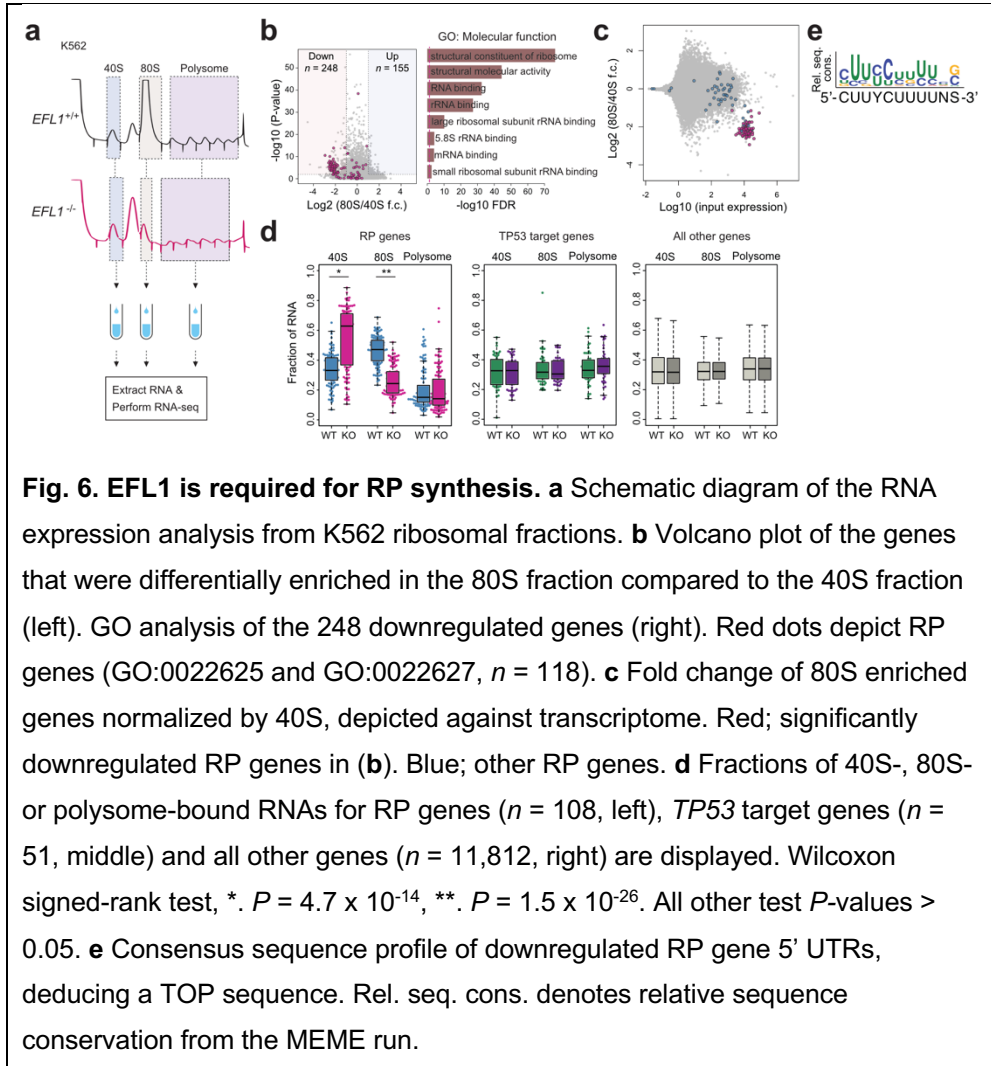
327

328

329 **Screening downstream factors of EFL1 dysfunction**

330 To further investigate the features of downstream genes that are strongly
331 affected by the reduced EFL1 function, we performed RNA-seq on the total
332 RNA, 40S-, 80S- and polysome-bound RNAs from wild type and *EFL1*^{-/-}
333 K562 cells (Fig. 6a; Fig. S20). The 60S-bound RNAs were not analyzed as it
334 is unlikely that the large subunit will bind with RNA by itself. The 248 genes
335 that were decreased in the 80S-bound fraction compared to the 40S-bound
336 fraction in the mutant cells were extracted. A gene ontology analysis
337 suggests that RP genes (GO:0003735) were the major constituents of the
338 genes that were reduced by the absence of *EFL1* ($P_{adj} = 5.2 \times 10^{-77}$,
339 adjusted by the Benjamini-Hochberg method; Fig. 6b-c). There was no
340 significantly enriched gene group in the increased gene set. The fractions of
341 the transcripts bound by 40S-, 80S-, or polysome differed substantially for
342 the RP genes in the absence of *EFL1* ($P < 1.0 \times 10^{-13}$ for differences in both
343 40S- and 80S-bound transcripts, Wilcoxon signed-rank test), whereas the
344 *TP53* target genes and all other genes did not show such a change (Fig. 6d,
345 $P > 0.05$, Wilcoxon signed-rank test). Next, we compared whether transcript
346 sizes (Fig. S21), expression levels, or consensus sequence elements in the
347 5' UTRs may serve as a factor that enabled RP-specific regulation. Notably,
348 highly-expressed RP transcripts with a terminal oligo-pyrimidine (TOP)
349 element (5'-CUUYCUUUUNS-3') were specifically altered (Fig. 6e; Fig. S22;
350 $P = 6.9 \times 10^{-7}$). This result revealed that, among all the genes in the

351 genome, 80S ribosome assembly of RP transcripts containing a TOP
 352 element were heavily dependent on the normal EFL1 function.
 353



354

355

356 **Discussion**

357

358 We identified and described a unique bone marrow-specific somatic UPD
359 event that preferentially selects cells with *EFL1* alleles of a weaker severity.
360 Although other parts of the body may suffer from biallelic variants in *EFL1*,
361 composed of more damaging one and the milder one, the hematological
362 system was partially rescued by a somatic UPD resulting in a homozygous
363 *EFL1*^{p.Thr1069Ala} with a weaker severity. We provided evidence suggesting that
364 the majority of the cells that carry *EFL1*^{p.Thr1069Ala} in a homozygous manner is
365 still pathogenic. We hypothesize that a somatic UPD in the patients could
366 occur and be detected because of the dynamic nature of bone marrow,
367 where the whole stem cell can be potentially replaced by a few clones.
368 Indeed, the somatic UPD was not detected in other solid organs or tissues
369 that were available for investigation. Two lines of evidence suggest
370 infrequent LOH events in the *EFL1* locus in normal populations (2.7-7.7 x
371 10⁻⁴; see Results). The odds of having all the p.Thr1069Ala and p.His30Arg
372 variants and the LOH by UPD in the *EFL1* locus for one person by chance is
373 roughly estimated as 1 in 3 trillion, indicating that detectable UPD is not an
374 independent event but is associated with the biallelic *EFL1* variants. It is still
375 not clear if the *EFL1* dysfunction somehow contributed to the occurrence of
376 UPD, causing the resulting clone to be expanded by positive selection.
377 Nevertheless, the degree of mosaicism did not seem to directly determine
378 clinical severity (Fig. S11). One could further delineate a more accurate

379 temporal and spatial occurrence of the event if additional clinical samples
380 become available.

381 Several lines of evidence from our experiments suggest that
382 although p.Thr1069Ala is the mildest among the variants that we found, it is
383 still functional and hypomorphic: (1) the parents of patients that were
384 heterozygous for *EFL1*^{p.Thr1069Ala} were asymptomatic, whereas the patients
385 carried the variant in a homozygous status in their bone marrow and
386 showed the pathology; (2) a ribosome profiling assay using a variant allele
387 partially rescued the 80S assembly problem, whereas the wild type allele
388 completely rescued it (Fig. 3); (3) *efl1* MO-treated zebrafish were partially
389 rescued by the variant-containing RNA (Fig. 4); and (4) *Efl1*^{m/-} mice
390 displayed an SDS-like phenotype, which was of an intermediate severity
391 relative to the *Efl1*^{-/-} and *Efl1*^{+/-} mice (Fig. 5). It is notable that although our
392 mouse model successfully phenocopied most of the SDS features, the
393 genotype was not in complete concordance with that of human patients. Our
394 mouse model with *Efl1*^{m/m} did not show significant phenotypes, whereas
395 human patients with bone marrow specific homozygous *EFL1*^{p.Thr1069Ala} by
396 somatic UPD still had hematological abnormalities such as anemia and
397 neutropenia. This discrepancy between the two species is not rare^{23,24}, and
398 it again underscores differences in tolerance to a given variant, perhaps due
399 to different physiological and genetic systems, which is critical in modeling
400 human clinical features in mice.

401 Nonetheless, we demonstrated that the altered function of *EFL1*
402 specifically influenced the translation of RP genes containing a TOP element
403 in the 5' UTR, which led to a mechanistic mimicry of Diamond-Blackfan
404 anemia, which is another ribosomopathy caused by insufficient RP
405 doses^{25,26}. The activation of TP53 is considered as a targetable downstream
406 pathway that leads to SDS or a DBA phenotype²⁷⁻²⁹. However, our data
407 suggest that the loss of *EFL1* does not induce TP53 activation, which is
408 consistent with previous studies of the zebrafish *slds* model and DBA (Fig.
409 6d)^{30,31}.

410 It is known that LARP1 directly binds to the TOP element of RP
411 genes to repress translation in a phosphorylation-dependent manner and
412 that mTOR partially regulates LARP1 phosphorylation^{32,33}. To determine if
413 we could utilize this pathway to de-repress RP translation and rescue the
414 SDS phenotype in the animal models, we considered a molecular signaling
415 pathway that may regulate RP gene translation through the TOP element.
416 However, both LARP1 binding to RP TOP elements and mTOR signaling
417 were unchanged in the mutant cells, suggesting an alternative mechanism
418 that may regulate RP translation (data not shown).

419 Here, we demonstrated a mechanism by which biallelic variants of
420 *EFL1* phenocopied classical SDS in three unrelated patients. The bone
421 marrow-specific somatic UPD in these patients mitigated the potentially
422 catastrophic hematological phenotype by homozygosing the less damaging
423 variant (*EFL1*^{p.Thr1069Ala}). We demonstrated that defective *EFL1* caused

424 impaired 80S ribosomal assembly and that the zebrafish and mouse models
425 displayed similar features to humans through the alteration of 80S ribosome
426 assembly of RP transcripts. An extensive search of such SDS patients may
427 provide more insight into the development of somatic mosaicism and
428 subsequent molecular cascades that may lead to new avenues of treatment
429 for ribosomopathy.
430

431 **Materials and methods**

432

433 *Patient recruitment and sampling*

434 Patient enrollment and sampling were conducted under the approval of the
435 Institutional Review Board of Seoul National University Hospital (IRB number:
436 H-1408-014-599). Patients or their parents were provided an informed
437 consent for genetic testing and collecting blood, buccal swab, scalp hair, urine
438 and clipped nails. Biopsy samples of I-1 (esophagus, stomach, duodenum,
439 colon and liver) were retrieved from the Department of Pathology of Seoul
440 National University for a research purpose.

441

442 *Whole exome sequencing and variant calling*

443 Trio whole exome sequencing (WES) was performed on one family (I-1, I-2,
444 and I-3) and singleton WES for two families (II-1 and III-1) at Theragen Etex
445 (Suwon, Korea) using genomic DNA extracted from whole blood. Exome was
446 captured using SeqCap EZ Exome v2 Kit (Roche Sequencing, Madison, WI)
447 or SureSelect Human All Exon V5 (Agilent Technologies, Santa Clara, CA)
448 and sequenced by HiSeq 2500 or HiSeq 4000 (Illumina, Inc., San Diego, CA).
449 Paired-end sequencing was performed with read lengths of 75 or 100 base
450 pairs. The raw reads were aligned by BWA MEM software³⁴. Variants were
451 called by Samtools and annotated by in-house pipeline and SnpEff³⁴⁻³⁶.

452

453 *Single nucleus SNP microarray*

454 Nuclei of frozen bone marrow cells from I-1, where a majority of the cells were
455 disrupted during freezing, were prepared and collected manually with a
456 pipette under a phase-contrast microscope. Buccal swab of III-1 was
457 resuspended in 1 ml of PBS and centrifuged at 300 g for 3 min. Supernatant
458 was discarded and pellet was resuspended in PBS. This suspension was
459 moved to a 100 ml cell culture dish. Single cells were manually picked up with
460 a pipette under a phase-contrast microscope. These single cells or nuclei
461 were whole-genome amplified by a REPLI-g Single Cell Kit (Qiagen, Venlo,
462 the Netherlands) for 3 hours. Amplified genomes were genotyped by Infinium®
463 OmniExpress-24 v1.2 (Illumina, Inc.).

464

465 *Sample-barcoded amplicon sequencing*

466 Genomic DNAs extracted from multiple individuals and tissues were PCR
467 amplified with primers shown in Table S6, with following condition: 3 min at
468 95°C, followed by 20 cycles (30 sec at 95°C, 30 sec at 57°C, and 20 sec at
469 72°C), and a final extension at 5 min at 72°C. Barcoded PCRs were
470 performed with 1 µl of first PCR product as templates using tissue-specific
471 barcoded primers (Table S7). Same reverse, forward and reverse primers of
472 *EFL1*, *WDR76* and rs1044032 with Sanger sequencing were used for
473 barcoded PCR products, respectively. The second PCR condition was: 3 min
474 at 95°C, followed by 20 cycles (30 sec at 95°C, 30 sec at 57°C, and 20 sec
475 at 72°C), and a final extension at 5 min at 72°C.

476

477 *Molecular dynamics (MD) simulation of EFL1*

478 The initial atom coordinates for MD simulations were from the Protein Data
479 Bank accession number 5ANC⁷. Input files were prepared with PSFGEN,
480 SOLVATE, and IONIZE plug-ins of VMD³⁷. Each simulation used explicit TIP3
481 solvent and periodic boundaries. Each unit cell contained one molecule of the
482 entire preinitiation complex. The unit cells were ~210 Å x 180 Å x 190 Å in
483 size and contained ~700,000 atoms. Sodium and chloride were added to
484 make the total ionic strength 100 mM. MD simulations were performed in
485 triplicate (each 50 ns in length) with a CHARMM36 force field³⁸ using NAMD2
486³⁹ on the Bebop cluster of the Laboratory Computing Resource Center at
487 Argonne National Laboratory. MD simulations were run at P = 1 atm, T = 310
488 K, with a 1 fs integration time and a 12 Å cutoff distance. Nonbonded forces
489 were calculated every two steps and electrostatic forces were calculated
490 every four. Pressure and temperature were maintained using a Langevin
491 piston and bath. Atom coordinates were recorded every 10 ps. MD trajectories
492 were visualized and analyzed with VMD and PyMol.

493

494 *Polysome profiling*

495 To maintain the binding of mRNA to ribosome subunits, cycloheximide
496 (Sigma-Aldrich, St. Louis, MO) (100 ug/ml) was added to cell culture media
497 and incubated for 10 min at 37°C. After incubation, cells were washed with
498 cold PBS including cycloheximide (10 ug/ml) twice, then lysed with 1 ml of
499 polysome lysis buffer (20 mM HEPES pH 7.6, 5 mM MgCl₂, 125 mM KCl, 1%

500 NP-40, 2 mM DTT) supplemented with cycloheximide (100 ug/ml), protease
501 inhibitor cocktail (EDTA-free; Roche) and RNase inhibitor (Invitrogen,
502 Carlsbad, CA) on ice. Cell lysates were tumbled for 20 min at 4°C and
503 centrifuged at 13,200 rpm for 20 min. The supernatants were fractionated in
504 17.5-50% linear sucrose gradients by ultracentrifugation (35,000 rpm for 160
505 min) in a Beckman ultracentrifuge using SW41-Ti rotor. Gradients were eluted
506 with a gradient fractionator (Brandel, Gaithersburg, MD) and monitored with
507 a UA-5 detector (ISCO). Equal volume of each polysome fraction was used
508 for determining the level of eIF6 by Western blot analysis.

509

510 RNA sequencing from polysome fractions

511 RNA was extracted from polysome fractionation. RNA sequencing library was
512 constructed using a TruSeq stranded total RNA kit (Illumina Inc.) with rRNA
513 depletion. 100 bp paired-end sequencing was performed using HiSeq 2500,
514 producing >5 Gb for each sample. Transcripts with polysome-bound RNA
515 count >10 were selected and subjected to calculation of fractions of 40S-,
516 80S- or polysome-bound RNA molecules for a given gene.

517

518 *Zebrafish experiments*

519 Zebrafish embryos were co-injected with *efl1* morpholino (MO) and normal or
520 mutated human *EFL1* mRNA at 1-2 cell stage. To evaluate the rescue efficacy
521 of each co-injected *EFL1* mRNA, the number of neutrophils and primary
522 erythrocytes were assessed. For neutrophils, individual Sudan Black stained

523 cells in the caudal region of the embryo, posterior to the anal opening, were
524 counted and the absolute number of positive cells were used for phenotypic
525 comparison. For primary erythrocytes, the degree of o-dianisidine staining
526 was qualitatively compared using the percentage of o-dianisidine stained
527 embryos within the population, since it is not technically possible to count
528 individual erythrocytes.

529

530 *Efl1* mutant mouse strain construction, maintenance and experiments

531 All the mouse experiments were performed under the standard protocols
532 approved by IACUC (#17-0148-S1A0). *Efl1* knock-out (*Efl1*⁻) strain was
533 constructed by introducing a 10-base deletion in the 10th exon of the gene in
534 C57BL6/J strain using CRISPR/Cas9 system in Macrogen (Seoul, Korea).

535 One cell embryos were microinjected with two sgRNAs (5'-

536 ACTTCTTTAGGATTA AAAATTGG-3' and 5'-

537 CCGAGGACAGCGTGGGATATGGG-3') and Cas9 protein mixture,

538 incubated and transplanted into pseudopregnant recipient ICR mice. *Efl1*

539 knock-in (*Efl1*^{p.Thr1076Ala}) variant was generated in C57BL6/J in University of

540 Utah Mutation Generation and Analysis Core using two sgRNAs (5'-

541 GTTCTGGGTGCCGACCACGG-3' and 5'-GTGCAGGTACTCCTCCTCCG-

542 3') and in the presence of oligodeoxynucleotides which includes the

543 ACC>GCC change mimicking the p.Thr1069Ala and an *Mbol* site for

544 genotyping. Genotyping strategies of the wild type and mutant alleles are

545 described in supplemental Methods. For phenotypic evaluations, wild type

546 and mutant mice from the same litter were sacrificed and dissected for
547 peripheral blood extraction, pancreas pathology and skeletal structure
548 analysis. 300 ul of peripheral blood was extracted from 35-42-day animals
549 and subjected to a complete blood count and differential tests.
550

551 **Author contributions**

552 M. Choi, H.J. Kang, and H.H. Kim conceived the study. S. Lee and M. Choi
553 performed genetic analysis and statistical evaluations. C.H. Shin, S. Lee,
554 S.D. Jeong, H.H. Kim, J. Lee, and M. Choi performed molecular biology and
555 biochemistry experiments and assessed the results. J. Lee, S. Lee, S.J.
556 Son, M. Choi, and J.K. Seong performed mouse experiments. J.-D. Kim, A.-
557 R. Kim, and S.-W. Jin performed zebrafish experiments. C.R. Hong, J.S. Ko,
558 Y.B. Sohn, O.-H. Kim, J.M. Ko, T.-J. Cho, and H.J. Kang provided patient
559 care and generated clinical data. N.T. Wright, O. Kokhan, and T. Yoo
560 analyzed protein structure. M. Choi, S. Lee, C.H. Shin, C.R. Hong, J. Lee,
561 H.J. Kang, and H.H. Kim wrote the manuscript. All authors approved the
562 final version of the manuscript.

563

564 **Acknowledgements**

565 We appreciate the patients and families that participated in this study. We
566 thank Jung-Ah Kim and Hyoung-Jin Kim at Seoul National University
567 Hospital for collecting and interpreting hematological data and for
568 interpreting images. We thank the University of Utah Mutation Generation
569 and Detection Core for construction of the *Efl1* knock-in mice. This study
570 was partly supported by grants from the National Research Foundation of
571 Korea (2014M3C9A2064686, 2019R1A2C2010789 to M.C. and
572 2017R1A2A2A05069691 to H.H.K.) and National Science Foundation (REU
573 CHE-1062629 and RUI MCB-1607024) awards to N.T.W.. This research

574 was partly supported by Korea Mouse Phenotyping Project
575 (2013M3A9D5072550) of the Ministry of Science, ICT and Future Planning
576 through the National Research Foundation. OK gratefully acknowledges the
577 computing resources provided by Bebop, a high-performance computing
578 cluster operated by the Laboratory Computing Resource Center at Argonne
579 National Laboratory. The authors declare no competing financial interests.

580

581 **Abbreviations used:** CH, compound heterozygous; DBA, Diamond-
582 Blackfan anemia; LOH, loss of heterozygosity; RP, ribosomal protein; SDS,
583 Shwachman-Diamond syndrome; TOP, terminal oligo-pyrimidine; UPD,
584 uniparental disomy; VUS, variants of unknown significances.

585

Table 1. Coverage depths and allele frequencies of *EFL1* variants

| Patient | Variant in <i>EFL1</i> (M: maternal origin, P: paternal, or U: unknown) | Method | Allele coverage depths (ref. allele:non-ref. allele) (% non-ref. allele) | | | AF in gnomAD | |
|---------|---|---------------|--|-------------------------|-------------------------|----------------------|----------------------|
| | | | Patient | Mother | Father | Overall | East Asian |
| I-1 | p.Thr1069Ala (M) | WES | 10:64 (86.5%) | 39:40 (50.1%) | 33:0 (0%) | 3.2×10^{-5} | 1.7×10^{-4} |
| | | Amplicon seq. | 23,914:131,714 (84.6%) | 63,582:63,954 (50.1%) | 121,502:507 (0.4%) | | |
| | p.Gly827TrpfsTer13 (P) | WES | 22:2 (8.3%) | 27:0 (0%) | 9:14 (60.9%) | 0 | 0 |
| | | Amplicon seq. | 243,610:43,042 (15.0%) | 505,158:74 (0.01%) | 221,532:218,976 (49.7%) | | |
| II-1 | p.Thr1069Ala (U) | WES | 15:59 (79.7%) | N/A | N/A | 3.2×10^{-5} | 1.7×10^{-4} |
| | p.His30Arg (U) | WES | 127:22 (14.8%) | N/A | N/A | 1.8×10^{-5} | 5.1×10^{-5} |
| III-1 | p.Thr1069Ala (P) | WES | 43:30 (41.1%) | N/A | N/A | 3.2×10^{-5} | 1.7×10^{-4} |
| | | Amplicon seq. | 135,196:149,160 (52.5%) | 189,517:1,786 (0.9%) | 87,347:85,317 (49.4%) | | |
| | p.His30Arg (M) | WES | 74:43 (36.8%) | N/A | N/A | 1.8×10^{-5} | 5.1×10^{-5} |
| | | Amplicon seq. | 25,316:22,680 (47.3%) | 119,382:121,508 (50.4%) | 41,684:76 (0.2%) | | |

588 **References**

- 589 1 Boocock, G. R. *et al.* Mutations in SBDS are associated with
590 Shwachman-Diamond syndrome. *Nat Genet* **33**, 97-101,
591 doi:10.1038/ng1062 (2003).
- 592 2 Shimamura, A. Shwachman-Diamond syndrome. *Semin Hematol* **43**,
593 178-188, doi:10.1053/j.seminhematol.2006.04.006 (2006).
- 594 3 Dror, Y. *et al.* Draft consensus guidelines for diagnosis and treatment
595 of Shwachman-Diamond syndrome. *Ann N Y Acad Sci* **1242**, 40-55,
596 doi:10.1111/j.1749-6632.2011.06349.x (2011).
- 597 4 Kuijpers, T. W. *et al.* Hematologic abnormalities in Shwachman
598 Diamond syndrome: lack of genotype-phenotype relationship. *Blood*
599 **106**, 356-361, doi:10.1182/blood-2004-11-4371 (2005).
- 600 5 Dror, Y. & Freedman, M. H. Shwachman-Diamond syndrome: An
601 inherited preleukemic bone marrow failure disorder with aberrant
602 hematopoietic progenitors and faulty marrow microenvironment.
603 *Blood* **94**, 3048-3054 (1999).
- 604 6 Hashmi, S. K. *et al.* Comparative analysis of Shwachman-Diamond
605 syndrome to other inherited bone marrow failure syndromes and
606 genotype-phenotype correlation. *Clin Genet* **79**, 448-458,
607 doi:10.1111/j.1399-0004.2010.01468.x (2011).
- 608 7 Weis, F. *et al.* Mechanism of eIF6 release from the nascent 60S
609 ribosomal subunit. *Nat Struct Mol Biol* **22**, 914-919,
610 doi:10.1038/nsmb.3112 (2015).
- 611 8 Menne, T. F. *et al.* The Shwachman-Bodian-Diamond syndrome
612 protein mediates translational activation of ribosomes in yeast. *Nat*
613 *Genet* **39**, 486-495, doi:10.1038/ng1994 (2007).
- 614 9 Narla, A. & Ebert, B. L. Ribosomopathies: human disorders of
615 ribosome dysfunction. *Blood* **115**, 3196-3205, doi:10.1182/blood-
616 2009-10-178129 (2010).
- 617 10 Tan, Q. K. *et al.* Further evidence for the involvement of EFL1 in a
618 Shwachman-Diamond-like syndrome and expansion of the
619 phenotypic features. *Cold Spring Harb Mol Case Stud* **4**,
620 doi:10.1101/mcs.a003046 (2018).
- 621 11 Stepensky, P. *et al.* Mutations in EFL1, an SBDS partner, are
622 associated with infantile pancytopenia, exocrine pancreatic
623 insufficiency and skeletal anomalies in a Shwachman-Diamond like
624 syndrome. *J Med Genet* **54**, 558-566, doi:10.1136/jmedgenet-2016-
625 104366 (2017).
- 626 12 Tummalala, H. *et al.* DNAJC21 Mutations Link a Cancer-Prone Bone
627 Marrow Failure Syndrome to Corruption in 60S Ribosome Subunit
628 Maturation. *Am J Hum Genet* **99**, 115-124,
629 doi:10.1016/j.ajhg.2016.05.002 (2016).
- 630 13 Dhanraj, S. *et al.* Biallelic mutations in DNAJC21 cause Shwachman-
631 Diamond syndrome. *Blood* **129**, 1557-1562, doi:10.1182/blood-2016-
632 08-735431 (2017).

- 633 14 Carapito, R. *et al.* Mutations in signal recognition particle SRP54
634 cause syndromic neutropenia with Shwachman-Diamond-like
635 features. *J Clin Invest* **127**, 4090-4103, doi:10.1172/JCI92876 (2017).
- 636 15 Tan, S. *et al.* EFL1 mutations impair eIF6 release to cause
637 Shwachman-Diamond syndrome. *Blood* **134**, 277-290,
638 doi:10.1182/blood.2018893404 (2019).
- 639 16 Finch, A. J. *et al.* Uncoupling of GTP hydrolysis from eIF6 release on
640 the ribosome causes Shwachman-Diamond syndrome. *Genes Dev* **25**,
641 917-929, doi:10.1101/gad.623011 (2011).
- 642 17 Chase, A. *et al.* PRR14L mutations are associated with chromosome
643 22 acquired uniparental disomy, age-related clonal hematopoiesis and
644 myeloid neoplasia. *Leukemia* **33**, 1184-1194, doi:10.1038/s41375-
645 018-0340-5 (2019).
- 646 18 Dubois, V. *et al.* Pretransplant HLA mistyping in diagnostic samples of
647 acute myeloid leukemia patients due to acquired uniparental disomy.
648 *Leukemia* **26**, 2079-2085, doi:10.1038/leu.2012.68 (2012).
- 649 19 Roberts, J. L. *et al.* CD45-deficient severe combined
650 immunodeficiency caused by uniparental disomy. *Proc Natl Acad Sci*
651 *U S A* **109**, 10456-10461, doi:10.1073/pnas.1202249109 (2012).
- 652 20 Swensen, J. J. *et al.* Sickle cell disease resulting from uniparental
653 disomy in a child who inherited sickle cell trait. *Blood* **116**, 2822-2825,
654 doi:10.1182/blood-2010-05-284331 (2010).
- 655 21 Lek, M. *et al.* Analysis of protein-coding genetic variation in 60,706
656 humans. *Nature* **536**, 285-291, doi:10.1038/nature19057 (2016).
- 657 22 Loh, P. R. *et al.* Insights into clonal haematopoiesis from 8,342 mosaic
658 chromosomal alterations. *Nature* **559**, 350-355, doi:10.1038/s41586-
659 018-0321-x (2018).
- 660 23 el-Amraoui, A. *et al.* Human Usher 1B/mouse shaker-1: the retinal
661 phenotype discrepancy explained by the presence/absence of myosin
662 VIIA in the photoreceptor cells. *Hum Mol Genet* **5**, 1171-1178,
663 doi:10.1093/hmg/5.8.1171 (1996).
- 664 24 Liao, B. Y. & Zhang, J. Null mutations in human and mouse orthologs
665 frequently result in different phenotypes. *Proc Natl Acad Sci U S A* **105**,
666 6987-6992, doi:10.1073/pnas.0800387105 (2008).
- 667 25 Draptchinskaia, N. *et al.* The gene encoding ribosomal protein S19 is
668 mutated in Diamond-Blackfan anaemia. *Nat Genet* **21**, 169-175,
669 doi:10.1038/5951 (1999).
- 670 26 Khajuria, R. K. *et al.* Ribosome Levels Selectively Regulate
671 Translation and Lineage Commitment in Human Hematopoiesis. *Cell*
672 **173**, 90-103 e119, doi:10.1016/j.cell.2018.02.036 (2018).
- 673 27 Danilova, N., Sakamoto, K. M. & Lin, S. Ribosomal protein S19
674 deficiency in zebrafish leads to developmental abnormalities and
675 defective erythropoiesis through activation of p53 protein family. *Blood*
676 **112**, 5228-5237, doi:10.1182/blood-2008-01-132290 (2008).
- 677 28 McGowan, K. A. *et al.* Ribosomal mutations cause p53-mediated dark
678 skin and pleiotropic effects. *Nat Genet* **40**, 963-970,

- 679 doi:10.1038/ng.188 (2008).
- 680 29 Elghetany, M. T. & Alter, B. P. p53 protein overexpression in bone
681 marrow biopsies of patients with Shwachman-Diamond syndrome has
682 a prevalence similar to that of patients with refractory anemia. *Arch*
683 *Pathol Lab Med* **126**, 452-455, doi:10.1043/0003-
684 9985(2002)126<0452:PPOIBM>2.0.CO;2 (2002).
- 685 30 Provost, E. *et al.* Ribosomal biogenesis genes play an essential and
686 p53-independent role in zebrafish pancreas development.
687 *Development* **139**, 3232-3241, doi:10.1242/dev.077107 (2012).
- 688 31 Ludwig, L. S. *et al.* Altered translation of GATA1 in Diamond-Blackfan
689 anemia. *Nat Med* **20**, 748-753, doi:10.1038/nm.3557 (2014).
- 690 32 Tcherkezian, J. *et al.* Proteomic analysis of cap-dependent translation
691 identifies LARP1 as a key regulator of 5'TOP mRNA translation.
692 *Genes Dev* **28**, 357-371, doi:10.1101/gad.231407.113 (2014).
- 693 33 Fonseca, B. D. *et al.* La-related Protein 1 (LARP1) Represses
694 Terminal Oligopyrimidine (TOP) mRNA Translation Downstream of
695 mTOR Complex 1 (mTORC1). *J Biol Chem* **290**, 15996-16020,
696 doi:10.1074/jbc.M114.621730 (2015).
- 697 34 Li, H. & Durbin, R. Fast and accurate long-read alignment with
698 Burrows-Wheeler transform. *Bioinformatics* **26**, 589-595,
699 doi:10.1093/bioinformatics/btp698 (2010).
- 700 35 Li, H. *et al.* The Sequence Alignment/Map format and SAMtools.
701 *Bioinformatics* **25**, 2078-2079, doi:10.1093/bioinformatics/btp352
702 (2009).
- 703 36 Cingolani, P. *et al.* A program for annotating and predicting the effects
704 of single nucleotide polymorphisms, SnpEff: SNPs in the genome of
705 *Drosophila melanogaster* strain w1118; iso-2; iso-3. *Fly (Austin)* **6**, 80-
706 92, doi:10.4161/fly.19695 (2012).
- 707 37 Humphrey, W., Dalke, A. & Schulten, K. VMD: visual molecular
708 dynamics. *J Mol Graph* **14**, 33-38, 27-38, doi:10.1016/0263-
709 7855(96)00018-5 (1996).
- 710 38 Best, R. B. *et al.* Optimization of the additive CHARMM all-atom
711 protein force field targeting improved sampling of the backbone phi,
712 psi and side-chain chi(1) and chi(2) dihedral angles. *J Chem Theory*
713 *Comput* **8**, 3257-3273, doi:10.1021/ct300400x (2012).
- 714 39 Phillips, J. C. *et al.* Scalable molecular dynamics with NAMD. *J*
715 *Comput Chem* **26**, 1781-1802, doi:10.1002/jcc.20289 (2005).
- 716

717